NAVAL POSTGRADUATE SCHOOL
Monterey, California

THESIS

LASER DAMAGE TO SPHERICAL TARGETS

by

Charles O. Stephenson

June 1985

Thesis Advisor: F. Schwirzke

SECURITY CLASSIFICATION OF THIS PAGE *(When Data Entered)*

REPORT DOCUMENTATION PAGE

READ INSTRUCTIONS BEFORE COMPLETING FORM

1. REPORT NUMBER	2. GOVT ACCESSION NO. / 3. RECIPIENT'S CATALOG NUMBER
4. TITLE *(and Subtitle)*: Laser Damage To Spherical Targets	5. TYPE OF REPORT & PERIOD COVERED: Master's Thesis, June 1985
	6. PERFORMING ORG. REPORT NUMBER
7. AUTHOR(s): Charles Otto Stephenson	8. CONTRACT OR GRANT NUMBER(s)
9. PERFORMING ORGANIZATION NAME AND ADDRESS: Naval Postgraduate School, Monterey, California 93943-5100	10. PROGRAM ELEMENT, PROJECT, TASK AREA & WORK UNIT NUMBERS
11. CONTROLLING OFFICE NAME AND ADDRESS: Naval Postgraduate School, Monterey, California 93943-5100	12. REPORT DATE: June 1985
	13. NUMBER OF PAGES: 61
14. MONITORING AGENCY NAME & ADDRESS *(if different from Controlling Office)*	15. SECURITY CLASS. *(of this report)*
	15a. DECLASSIFICATION/ DOWNGRADING SCHEDULE

16. DISTRIBUTION STATEMENT *(of this Report)*

Approved for public release; distribution is unlimited.

17. DISTRIBUTION STATEMENT *(of the abstract entered in Block 20, if different from Report)*

18. SUPPLEMENTARY NOTES

19. KEY WORDS *(Continue on reverse side if necessary and identify by block number)*

Unipolar Arcing, Laser Target Damage

20. ABSTRACT *(Continue on reverse side if necessary and identify by block number)*

Previous research has investigated laser beam interaction with flat surfaces. Those studies have generated theoretical foundations for cratering, plasma formation and expansion, and electric and magnetic field dynamics. This study applies previously developed theory to understanding damage to spherical targets of 1 millimeter diameter and smaller. The targets analyzed were irradiated on one side with 300 picosecond iodine laser pulses (6×10^{15} W/cm). Direct laser beam damage and surface damage to areas remote from the focal spot

DD FORM 1 JAN 73 1473 EDITION OF 1 NOV 65 IS OBSOLETE

S N 0102-LF-014-6601

SECURITY CLASSIFICATION OF THIS PAGE *(When Data Entered)*

were analyzed. Time-resolved pinhole photography , x-ray spectroscopy, and electron microscope photography were used to determine sequence, mode and severity of damage. Finally, a model for the creation and spread of the laser-produced plasma around the sphere is formulated, taking into account plasma pressure gradients, magnetic fields and hot-electron transport.

Laser Damage To Spherical Targets

by

Charles O. Stephenson
Lieutenant, United States Navy
B.S., United States Naval Academy, 1978

Submitted in partial fulfillment of the
requirements for the degree of

MASTER OF SCIENCE IN PHYSICS

from the

NAVAL POSTGRADUATE SCHOOL
June 1985

ABSTRACT

Previous research has investigated laser beam interaction with flat surfaces. Those studies have generated theoretical foundations for cratering, plasma formation and expansion, and electric and magnetic field dynamics.

This study applies previously developed theory to understanding damage to spherical targets of 1 millimeter diameter and smaller. The targets analyzed were irradiated on one side with 300 picosecond iodine laser pulses (6×10^{15} W cm^{-2}). Direct laser beam damage and surface damage to areas remote from the focal spot were analyzed. Time-resolved pinhole photography, x-ray spectroscopy, and electron microscope photography were used to determine sequence, mode and severity of damage. Finally, a model for the creation and spread of the laser-produced plasma around the sphere is formulated, taking into account plasma pressure gradients, magnetic fields and hot-electron transport.

TABLE OF CONTENTS

LIST OF TABLES

LIST OF FIGURES

ACKNOWLEDGEMENTS

I wish to acknowledge the work performed by personnel of the Max-Planck Institute for Quantum Optics in Garching, Federal Republic of Germany. Through Professor Schwirzke, they provided the laser-damaged targets studied in this report, along with photographs and a report of their experimental findings.

Special thanks also go to Bob Sanders and Tom Kellogg for their valuable technical assistance, and to Professors Schwirzke and Cooper for their guidance through this project.

I. INTRODUCTION AND BACKGROUND

Since the discovery of the laser in the early 1960's, the industrial, military and academic communities have conducted extensive studies into the interaction of beam radiation with various materials. The effects of high power lasers on target surfaces include heating, melting, vaporization, emission of a plasma made up of charged particles, and electromagnetic phenomena.

Over the past two decades, extensive research has been devoted to the study of phenomena associated with the resulting laser-produced plasmas. Early investigations into laser induced electron emissions were conducted by William I. Linlor in 1962 [Ref. 1]. Discovery of self-generated magnetic fields were made independently by Korobkin and Serov [Ref. 2] and Stamper [Ref. 3] in the late 1960's. Since then, a multitude of studies have been conducted at the Naval Postgraduate School (NPS) and elsewhere dealing with laser-plasma asscciated self-generated magnetic fields, currents, hot-electron transport, x-ray emission and other related topics.

However, those studies were based on laser interactions with flat surfaces. With the current interest in laser induced fusion, the study of laser interaction on spherical targets of less than one millimeter diameter is necessary. Using the Asterix III laser at the Max-Planck Institute for Quantum Optics in Garching, Federal Republic of Germany, small steel and vanadium spheres were irradiated at intensities of 6×10^{15} W cm^{-2} .

This study examines the damage to these targets. From the data and photographs taken at the time of the original experiments [Ref. 4], coupled with analysis of damage mode

and distribution, a model is formulated for the dynamics of the plasma damage.

This thesis is divided into six sections. Section II discusses theory relevant to direct laser damage and the plasma damage which occurs in areas remote from the focal spot, along with other plasma related phenomena. Section III describes the experimental arrangement, both that of the team at the Max-Planck Institute and analytical methods used for this study. Section IV contains the data and results, and the components of the total model proposed in the Summary and Conclusions write-up, Section V and VI.

II. THEORY

High power laser beams directly damage target surfaces by a variety of thermal, impulse and electrical effects. The absorption of the incident energy creates a hot plasma, which spreads beyond the shot crater to cause extensive surface ablation by thermal evaporation, ion sputtering and unipolar arcing.

A. DIRECT LASER BEAM DAMAGE

Of the different damage mechanisms caused by lasers, thermal damage is the most significant in the area of the focal spot. The damage is due to the absorption of the laser photon energy by the surface atoms, resulting in melting, vaporization and ionization. The vaporized and ionized atoms create a hot plasma gas, which carries away with it target material, leaving a crater on the surface at the focal spot. The size and depth of the crater is a function of the focal spot size, the laser intensity, and the pulse duration.

A second mechanism by which a laser damages a target is impulsive loading. The rapid expulsion of matter from the shot crater, blow-off, has momentum. The laws of physics require that as the blow-off occurs, an equal but opposite force be exerted on the target to conserve momentum. Impulse is generally not a significant damage mechanism on a macroscopic scale.

A laser beam, being electromagnetic in nature, contains intense electric and magnetic fields. In addition, the ionization of the target surface and the temperature gradients also produce self generated currents and magnetic

fields. These electromagnetic fields determine, to a large degree, the dynamics of the expanding ionized plasma gas and the liberated electrons.

B. PLASMA DAMAGE

Any damage to the surface of a target outside of the shot crater is due to plasma surface interaction. Mechanisms effecting laser plasma are difficult to discuss in isolation, since they are all interrelated. The laser creates a plasma of ions and hot electrons, which cause currents, which cause magnetic fields, which cause the hot electrons to be reflected back to the surface, which causes the creation of more plasma and the emission of x-rays. The magnetic fields also restrict the plasma flow, while the plasma is causing arcing to the surface. Each of these effects will be discussed independently in the following sections.

1. Unipolar Arcing

"Unipolar arcing represents the most damaging and non-uniform laser-plasma-surface interaction process since the energy available in the plasma concentrates towards the cathode spots." [Ref. 5] During laser impact, the surface is vaporized, creating an electron and ion plasma. In addition, a space charge sheath covers a portion of the target due to electrons making large amplitude orbits, but confined by the target potential, and electrons escaping from the target completely, as discussed by Ebrahim et al [Ref. 6]. Unipolar arcing is a purely electrical plasma-surface interaction process which leads to crater formation, called laser pitting. It occurs whenever a hot plasma of sufficiently high electron temperature interacts with a conducting wall. Many micro-arcs burn between the

surface and the variations in the sheath potential. The surface acts as both anode and cathode in the arcing process, due to localized variations in surface potential relative to the plasma. The plasma energy is concentrated onto a single spot of micrometer dimensions, causing small craters. The material ejected from the crater in small jets leads to ripples in the critical density contour and highly localized shock waves which further soften the surface.

The mechanisms of unipolar arcing, including detailed equations, diagrams and photographs is covered extensively by Schwirzke in reference 7, so it will be only briefly summarized here. The quasi-neutrality requirement for a plasma leads to the formation of a sheath between the target and the plasma. The plasma loss rate to the wall is controlled by the sheath potential, (V_f). Arcing occurs if the sheath potential increases to the point where it can ignite and sustain an arc. A current loop is set up, and the arc burns with the surface acting as both anode and cathode (Figures B.1 and B.2). A perturbation in the sheath may result in an ion density increase above the cathode spot, resulting in a potential sufficient to drive the current causing the arc (Figure B.3). The increased pressure above the cathode spot also causes a radial electric field, E_r, in a ring-like area above the spot. This radial electric field reduces the plasma potential in a ring around the cathode spot, which allows the electrons in the high energy tail of the maxwellian distribution to reach the surface, thus closing the current loop for the unipolar arc.

The size of the crater is a function of burn time (i.e. the duration of the plasma over the surface and/or the duration of the perturbation necessary to sustain the arc) and the sheath potential, which is a function primarily of the hot electron temperature. Whenever there is a plasma,

there is arcing; one has never been observed without the other. The size, density and superposition of arcs can be used as indicators of the plasma dynamics for an experiment.

2. Hot Electron Deposition

While electromagnetic energy may liberate electrons in a number of ways, resonance absorption accounts for the vast majority of fast electrons emitted from an area irradiated by a laser pulse. In resonance absorption, incoming electromagnetic waves are linearly converted to outgoing plasma waves near the critical layer. These in turn transfer their energy to an outgoing stream of fast electrons. Return current follows a different path such that it produces a current loop and finite magnetic field.

Hot electrons may carry up to 30% of the absorbed laser energy away from the focal spot [Ref. 8]. Suprathermal electrons are found to be nearly collisionless with the surrounding plasma, which expands at velocities of the order of 10^8 cm/sec. A significant fraction of the electrons are reflected at the plasma cloud boundary, depositing their energy on the target away from the focal spot.

The exact trajectory of the electrons is complicated by intense magnetic and electric fields. Amiranoff et al carried out quantitative analysis of the amount of energy carried away from the laser impact area by suprathermal electrons on several of the world's research lasers, including the Asterix III iodine laser used in this experiment (Table I) [Ref. 9]. An appreciation for the significance of hot electron transport may be gained when the fact that the energy carried away by the suprathermal electrons may sometimes exceed the energy deposited under the focal spot is considered [Ref. 9].

Hot electrons execute large excursion orbits in the electrostatic fields of the target along the outer edge of a rapidly expanding ion sheath. The expansion slows as the halo propagates outward. Forslund and Brackbill described how the halo would expand until the end of the laser pulse for larger targets [Ref. 10]. For smaller planar targets, they found that the halo would spread to the edge of the target, become stationary and bright momentarily, then go to the rear. These findings explain how a plasma sheath formed from a laser shot at a sherical target will spread around the sphere for the duration of the laser pulse. In all cases, the expansion terminated when the laser was shut off.

While many electrons return to the focal spot, many execute large excursion trajectories, returning back to the target at the leading edge of the outer sheath, resulting in the acceleration of fast ions and more or less uniform heating of the surface by the electrons, creating a plasma and causing x-rays to be emitted. The tendency of electrons to deposit at the edge of the ring is due to the toroidal magnetic fields in the plasma channeling the electrons to the edge of the plasma cloud. For a spherical target, if the pulse is of sufficient duration, the plasma clouds spread around the entire surface and meet 180 degrees from the shot impact area. Several interrelated effects will combine to make this rear surface one of extreme electron deposition. First, the magnetic fields will combine to make this an area of high magnetic flux, thus channeling the electrons to the surface better. Second, the plasma fronts will combine to make a very high pressure gradient, contributing to the magnetic fields. Furthermore, the area over which electron deposition occurs will be greatly reduced from a large area over an entire arc of the sphere to a single point on the rear of the sphere. This reduction in area will cause a dramatic increase in the electron flux,

further contributing to the fields. Lastly, the increased electron deposition will cause greater heating and ionization of the surface, resulting in a newly created plasma contributing its own pressure and field gradients to those of the laser produced plasma.

3. Magnetic Fields

The dynamics of laser produced self-generated magnetic fields have been extensively studied at NPS and elsewhere. In studies conducted by F. Schwirzke [Ref. 11], the dependence of the magnetic fields as a function of time, position, laser power density and ambient background pressure was examined. The magnetic fields were found to propagate at velocities approximately equal to those of the plasma fronts. The plasma temperature and density gradients were attributed to the mass difference between the heavy ions and light electrons. The strongest field production occurs at the edge of the focal spot where the temperature gradient is largest and at the front of expanding plasma where the pressure gradient is largest. Magnetic field intensities in the megagauss range have a significant effect on the density and temperature gradient distribution in the plasma (via $\vec{j} \times \vec{B}$).

The research conducted by McKee *et al* at NPS [Ref. 12] further investigated the dynamics of self-generated magnetic field associated with laser produced plasmas. The magnitude of the fields generated were found to depend greatly on ambient pressure. The current-density distribution produced the self-generated magnetic field via ($\vec{\nabla} \times \vec{B} = \mu_o \vec{j}$). The current flow in McKee's experiments was found to be toroidal. The overall equation which governs the self-generated magnetic fields is

$$\frac{\partial \vec{B}}{\partial t} = \frac{1}{\mu_o \sigma} \nabla^2 \vec{B} + \vec{\nabla} \times \left(\vec{V}_e \times \vec{B} \right) + \frac{k}{e n_e} \vec{\nabla} T_e \times \vec{\nabla} n_e$$

where v_e is the electron flow velocity, n_e is the electron density, T_e is the electron temperature, σ is the scalar electrical conductivity. The last term in the above equation is the source term

$$\vec{S} = \frac{k}{e n_e} \vec{\nabla} T_e \times \vec{\nabla} n_e$$

Examination of the source term shows that no field generation can occur unless ∇T_e and ∇n_e are nonparallel. The largest fields are generated during the laser heating of the plasma. However, since plasma is still being created after the end of the pulse, magnetic field generation and even field reversal may occur at some finite time after laser pulse termination.

Sakagami et al [Ref. 13] carried out research similar to that of Schwirzke and McKee, but also studied the effects of the trajectories of the electrons emitted by resonance absorption in addition to the magnetic fields resulting from thermoelectric mechanisms. The fields resulting from thermoelectric mechanisms were found to be toroidal in shape, as described by Schwirzke and McKee, while the magnetic fields resulting from resonance absorption were found to create a lobe pattern. The actual pattern of the magnetic fields around the focal spot was found to be a superposition of these two geometries. The magnetic fields were found to be frozen in the expanding plasma, and could survive for nanoseconds, even though the pulse duration was only 30 picoseconds.

Fabbro and Mora [Ref. 14] found that the dc toroidal magnetic fields account for the hot electron transport which leads to ring-like structures around the laser impact area. The rings were attributed to deposition of energy carried by electrons whose trajectory was governed by

$$M_e \frac{d\vec{v}}{dt} = -e\left(\vec{E} + \vec{\nabla} \times \vec{B}\right)$$

The higher the magnitude of the magnetic field, the longer time the electrons would spend in the corona, resulting in deposition of energy at greater distances from the laser focal spot. The rings of deposition were found to be typically on the order of one millimeter from the focal spot center.

Forslund and Brackbill found in their investigations [Ref. 10] that the electrons heated by resonant absorption of laser energy generate intense magnetic fields which rapidly spread from the edge of the laser spot to the edge of the target, become momentarily stationary, then move around to the back of the target (Figure B.4). The magnetic fields were found to transport convectively the hot electrons and confine a major portion of the deposited energy.

Stamper et al examined the extent of the magnetic fields generated [Ref. 3]. They determined that the large temperature gradients produced by lasers caused photoionization of the background gas. The photoionization resulted in large thermoelectric current flow in the gas, with corresponding magnetic field generation. That was also the finding of McKee, which accounts for the dependence on ambient pressure. Photoionization is complete out to a few millimeters, then rapidly decreases as the inverse square of the radius.

III. EXPERIMENTAL ARRANGEMENT

The targets analyzed for this thesis were the subject of experiments carried out by K. Eidmann et al at the Max-Planck Institute for Quantum Optics in Garching, Federal Republic of Germany [Ref. 4]. The objective of the original experiments was to determine the difference in hot-electron transport between supported and unsupported targets. The targets analyzed herein were retrieved from the bottom of the experiment chamber at conclusion of the experiment. Figure B.5 shows the experimental set-up, including the simple mechanism for release of unsupported targets and diagnostic apparatus. The targets were placed on a flexible steel ribbon, which was punched down using the snapper of a mouse trap. The inertia of the target sphere kept it from being snapped immediately away, resulting in its motion being only that of free fall. After two milliseconds, the laser is fired. In this time interval, the sphere would have moved approximately twenty micrometers, a negligible distance in relation to other dimensions of the experiment. The target spheres used were made of either solid vanadium or steel, and ranged in size from 320 to 1000 micrometers in diameter.

The laser used to irradiate the targets was the Asterix III iodine laser. The laser pulse was 100J/300 ps (full width at half-maximum), with a wavelength of 1.3 micrometers, and a focal spot diameter of 60 micrometers. The intensity corresponding to these specifications was 6×10^{15} W cm^{-2} .

A kα spectrometer and an x-ray pinhole camera were used to determine quantitatively the hot-electron energy deposited on the target sphere. A series of shadowgraphs

using a 3 ps exposure time and 1.95 ns interval was used to generate a time resolved sequence for each experiment. An electron spectrometer using no screen film was used to determine the energies of emitted electrons. Several pieces of cellulose nitrate (CN^-) film were affixed to the inner wall of the target chamber tc record fast ion emissions. Four different calorimeters at different angles with respect to the horizontal plane measured the x-ray emission from each target.

The results presented in reference 4 were used in the general analysis of these targets studied. However, several variables which would strongly influence quantitative results were unknown. These variables were target composition, laser pulse power and ambient background pressure inside the target chamber. Whether the targets were made of steel (or even exactly what type of steel) or vanadium would determine their thermodynamic characteristics, hardness and even the characteristics of the plasma produced. As determined by Schwirzke in reference 11, the ambient background pressure greatly effects how the plasma and magnetic fields propagate. Finally, as in all lasers, the pulse to pulse power varies; so for precise quantitative analysis, a measurement of the exact power of the pulse corresponding to a particular target would have to be known.

Target surface damage was then studied with the aid of an electron microscope. Low magnification photographs (X 100) were taken to be used as a reference for additional photographic mapping and also to give an overall impression of the damage. With the low magnification photograph in hand, detailed examination of regions which typified other modes or densities of damage could be carried out. The laser shot axis (i.e. crater) was always used as the reference, with all other points being measured radially as

degrees off shot axis. These high magnification photographs (up to X 5000) were used to determine unipolar arc size and density, surface flow patterns, and other general characteristic of the surface. Two photographic series were made to form detailed composites to study the radial progression of damage on different size targets from the shot crater to the rear pole of the sphere.

IV. DATA AND RESULTS

A total of five targets, varying in size from 570 micrometers to 1 millimeter in diameter, where examined. These targets were representative of the entire group, providing an adequate base on which to formulate a model for laser target damage to spherical targets. The following sections contain observations, data, and calculations, along with interpretations of the cause and effect of each phenomenon.

A. DIRECT LASER DAMAGE

The area of each sphere which sustained the direct laser pulse is obvious, due to the crater. Table II lists the data for the targets analyzed. Figures B.6-B.10a illustrate that the interior surfaces of the craters are essentially identical, having the smooth appearance of solidified liquid metal. Figure B.11 depicts the crater sizes of representative targets relative to the focal spot size to illustrate the extent of direct shot damage. The laser beam strikes the surface, then progressively vaporizes the target (Figure B.12). The variation in crater size is most likely due to fluctuations in the energy from pulse to pulse, which is characteristic of all high power lasers, and to possible variations in sphere composition.

The second point of note on the photographs is that molten metal is forced radially from the crater. In some cases, targets B and E, liquid metal covered the entire hemisphere of the shot, before its momentum carried it beyond the equator, leaving "fingers" of molten metal reaching around the edge. In three of the cases, targets A,

C and D, any liquid metal that did return to the surface of the sphere did so in the form of debris (Figure B.13). The factors which may determine if liquid metal spreads smoothly over the surface or is scattered in the form of debris are sphere composition and crater depth. Whether the spheres were made of vanadium or steel would determine the thermal characteristics of the material. The steepness of the crater walls would determine the trajectory at which the liquid material left the target. Spheres B and E appeared to have shallower craters than did spheres A, C and D.

B. UNIPOLAR ARCING

Unipolar arcing was found to be present over most of the surface of all of the spheres. The size and density of the arcs varied greatly as a function of the plasma dynamics over that particular spot. The main plasma, that created by the vaporization/ionization of the surface irradiated by the laser, spread radially from the focal spot. The plasma motion would be governed by the plasma pressure gradients, thermal velocities, and magnetic fields. It would continue to increase for the duration of the pulse (Figure B.14).

All surface area exposed to the plasma gas will experience arcing to some degree. The areas of large arcs and high arc density were covered by a plasma of very high sheath potential for a relatively long period (Figure B.15). The superposition of arcs means that one arc burned until it could no longer be sustained, then later, conditions requisite for arcing were once again met over that same spot (Figure B.16). If arcing is very dense, the molten metal from one arc may fill an adjacent arc crater. Areas of high density of arcing will also exhibit large amounts of debris from those arcs scattered about the surface. The areas over which little plasma spread experienced very light arc

damage, as can be seen on the back sides of targets A and B (Figure B.17). The arcs in this region are very small and widely spaced.

While the main plasma is spreading, hot electrons are being emitted from the shot crater, many of which execute orbits and deposit on the leading edge of the plasma. These impact on the surface, creating their own plasma, with associated pressure gradients and magnetic fields. The areas of hot electron deposition were determined by X-ray pinhole photographs. In the analysis of these spheres, the surface areas corresponding to those which emitted intense X-rays were pitted by dense unipolar arcing. Since this plasma was formed after the laser pulse plasma, analysis of the arc and flow patterns give a good indication of the overall time resolved plasma dynamics.

On the larger targets, this hot electron induced plasma occurred near the equator. On smaller targets, it occurred more towards the pole opposite the shot. Table III gives representative distributions based on X-ray photographs, Figure B.18, copied from reference 4 . An insight into the reason behind these distributions may be gained by noting the radial distance traveled by the plasma front. The velocity of the plasma front will be similar for all shots. Taking the distance traveled and dividing that by the pulse duration gives correct characteristic velocities for the plasma, within an order of magnitude. These calculations also agree with the shadowgraphs, Figure B.19 .

The X-ray photographs and shadowgraphs of the larger spheres show a great deal of activity at the equator, because that is as far as the plasma could travel before the pulse ended. On the intermediate size targets, the plasma had just enough time to reach the back, at which point the plasma fronts met, creating a denser plasma. In addition, this area would have been where the hot electrons associated

with the plasma fronts would have been deposited, contributing further to the plasma density. The electron deposition would be even further enhanced by the fact that the point 180 degrees from the shot axis would have been a magnetic maximum. On the smallest spheres, the plasma would have had time to spread beyond the confines of the sphere. There would be hot electron deposition on the rear surface, but since the plasma fronts do not exactly coincide with this surface, it would be somewhat less. This could account for the lower intensity of the 320 micrometer X-ray photograph. As no spheres of this size were available for analysis, the distribution and extent of damage cannot be verified.

The wave-like flow patterns on target A are away from the equator in both directions, with arc density decreasing with distance from the equator. This indicates that a dense plasma was emitted from the crater and spread as far as the equator (Figure B.22). The hot electrons created a plasma at the equator, which combined with the main plasma cloud to become even more dense (Figure B.23). When the laser pulse ended, the pressure gradient associated with the equatorial plasma became dominant, spreading radially in both directions until the plasma dissipated (Figure B.24). This model would account for the flows in both directions from the equator, and the higher arc density on the shot hemisphere. Target B exhibited the same type of flow patterns as A (Figure B.16), since the spheres are of identical dimension, except that all damage to the shot hemisphere has been concealed by the molten metal flow.

Target C provided some of the most striking evidence in support of this plasma dynamics model. The arcing is very dense in the area of the shot crater (Figure B.25). At the area 180 degrees from the shot axis, dense arcing occurred, but the flow direction is random (see center of Figure

B.26). Examination of areas approximately 135 degrees from the shot axis shows definite flow patterns away from the rear axis (Figure B.26). Due to the small size of the target, a magnetic maximum was created at the pole opposite the shot crater and this area also corresponded to the maximum expansion of the laser plasma cloud (Figure B.27). Hot electrons were deposited here, creating a dense plasma. This plasma then spread radially toward the shot crater until the laser pulse ended (Figure B.27a).

Another factor which may have contributed to the flow pattern on the rear surface of target C is shock waves created by the high velocity plasma fronts. As the plasma clouds spread around the sphere, they will collide at the pole opposite the crater (Figure B.28). The result will contribute to the high pressure gradients on the rear surface, until this pressure becomes dominant and spreads radially forward toward the shot crater, contributing to the organized flow patterns observed in Figure B.26 .

C. HOT ELECTRON TRANSPORT

The mechanics of hot electron transport are well understood, and covered in detail in the references cited in the theory section. To make an analysis of the ability of these electrons to create a plasma, it was necessary to determine the amount of energy they would deposit on the target surface. Reference 4 states that the observed spectrum of suprathermal electrons was in the energy range of 50 - 100 KeV. From Principles and Techniques of Radiation Hardening by N. J. Rudie [Ref. 15], it was calculated that these electrons would have a penetration depth of 8.3 - 26 micrometers. Therefore, they would penetrate just slightly into the surface, depositing their energy. If the reasoning of J. D. Hare et al is followed

[Ref. 8], the energy balance on the target would be approximately:

Energy onto target	100 J
Energy absorbed by target (30%)	30 J
Energy absorbed by ions (60% of absorbed)	18 J
Energy absorbed by hot electrons (30% of absorbed)	9 J
Energy used to preheat target (10% of absorbed)	3 J

Table III lists the calculated values of energy flux on the surface. The flux values were found to be on the order of magnitude of 10^{12} W/cm^2, which is sufficient for the creation of a plasma. These values are based on the model that 9 J of energy in the hot electrons was deposited over the area which emitted the x-rays, during a period equal to that of the laser pulse.

$$\frac{(9\ \text{J of energy in hot electrons})}{(\text{Area of Deposition}) \times (\text{Pulse duration})} = \text{INTENSITY}$$

The value for the 320 micrometer sphere is probably high, since the plasma would have spread beyond the rear surface of the sphere, as noted earlier.

The propagation velocity of the plasmas can be deduced by analysis of the X-ray photographs and the shadowgraphs. From the X-ray photographs, the radial velocity of the plasma from the laser impact area was calculated to be between 2.4 and 3.5 X 10^8 cm/sec (see Table IV). The propagation velocity of the hot-electron-produced plasma radially outward from the surface was determined from Figure B.19 to be between 3.8 and 4.2 X 10^6 cm/sec (see Table V). The difference between these plasma velocities and those calculated earlier is about two orders of magnitude. The difference may be explained by : (1) the observed halo is a dense layer of overlapping plasma jets rather than a uniform

expanding plasma front, and (2) the plasma is cooler than the laser-produced plasma, and therefore propagates more slowly. Although these calculations are extremely crude, the order of magnitude of the answers does agree with laser plasma velocities found elsewhere in the literature and does present a method for analysis of these velocities.

V. SUMMARY

To summarize the findings presented in the Data and Results section, the following sequence of events has been formulated. The sequence of the events is based on the target flow patterns, density and size of unipolar arcs, shadowgraphs, and x-ray photographs. The events are presented in the sequence in which it is believed that they occurred, but the times are only approximate.

EVENT 0 (time = 0)

The target is undamaged and unsupported (i.e. free falling). The laser is fired at time = 0.

EVENT 1 (time = 0 - .3 nsec)

The laser beam irradiates the target. The photon energy ionizes, then progressively melts and vaporizes the exposed critical layer. A plasma gas develops at the focal spot with very high temperature and pressure gradients. Hot electrons are emitted primarily due to resonant absorption. Some of the electrons escape, but many of them return at the focal spot, while others execute orbits and return at the leading edge of the plasma cloud. Strong magnetic fields in the megagauss range are created within the plasma. Powerful current loops are set up within the plasma and target surface. A potential sheath is created between the expanding plasma and the target surface, accompanied by unipolar arcing. Intense x-rays are emitted from the focal spot.

Event 2 (time = 0.3 - 2.3 nsec)

The laser pulse ends at time = 0.3 nsec. Due to the large pressure gradients, the plasma continues to expand at a velocity of the order of 10^8 cm s^{-1} . The expansion is restricted by the large magnetic fields now frozen in the expanding plasma. Areas of high electron deposition become hot, causing them to emit x-rays and create a plasma of their own. Liquid material from the shot crater begins to cover the shot hemisphere, either as debris or as a smooth flow.

EVENT 3 (time = approximate 2.3 nsec)

The laser plasma has reached the maximum extent of its expansion. On the 1.0 millimeter sphere, this occurs near the equator, 90° from the shot axis. The expansion is stopped by this point being the maximum extent to which the pressure gradient and magnetic field would allow it to expand, and also by the opposing pressure gradient of the plasma being created at the equator by the hot electron deposition. On the smaller spheres, the laser fronts will have collided at the rear pole, creating a high pressure gradient and shock waves. The magnetic field lines frozen in the expanding plasmas will also have combined, resulting in a large magnetic field. These combined effects will have a channeling effect for hot electrons, focussing them onto a single spot 180° from the focal spot. This high electron flux will result in highly localized surface heating, which will cause x-ray emission, plasma creation, and dense unipolar arcing.

EVENT 4 (time > 2.3 nsec)

The pressure of plasma gas over the areas of hot electron deposition becomes dominant over the laser produced plasma. On the 1.0 millimeter spheres, the pressure is greatest at the equator, causing flow toward both poles (i.e. the shot

crater and the pole 180° from the shot crater). On the smaller spheres, the newly created plasma gas will flow from the rear pole (180° from shot axis) toward the shot crater. The plasma flow direction will cause metal liquefied by unipolar arcing to orient itself in the direction of the flow. The creation of new plasma by hot electron deposition has essentially ceased by this time. The plasma present is expanding primarily under its own pressure gradients and magnetic fields. Unipolar arcing is still occurring, but the sheath potential and plasma pressure are dropping, so the arcing activity is decreasing.

EVENT 5 (time > 4.2 nsec)

All plasma pressure gradients continue to drop and the plasma clouds reach their maximum extent. The sheath potential drops below its critical value, causing unipolar arcing to cease. The liquid metal streams on the target surface cool, preserving the record of destruction. For these targets, the entire process is over in a few nanoseconds.

VI. CONCLUSIONS

As stated in the introduction, the purpose of this study was to determine the dynamics of laser target damage to spherical targets of a millimeter or less diameter. The model developed and proposed here includes no attempt at quantitative analysis, due to the number of experimental unknowns. However, utilizing available shadowgraphs and x-ray photographs, coupled with analysis of metal flow patterns and unipolar arc distribution on the target spheres, a plausible model of the sequence of damage was formulated. This model combines the complex interactions of thermal, electrodynamic and mechanical effects. The analysis of the actual damage demonstrated that the most significant macroscopic damage occurred at the focal spot due to direct thermal melting and vaporization of target material. In areas remote from the shot crater, extensive damage occurred due to unipolar arcing. The arc size and density were found to be a function of how dense the plasma was and how long it persisted over that particular spot. The flow patterns of the liquefied surface metal were used to support hypothesized dynamics of the plasmas.

The main difference between this experiment and those for the controlled fusion program is in the targets used. The controlled fusion program uses spheres of these sizes, but they are thin walled and filled with a deuterium-tritium gas. The laser power, irradiating the small sphere simultaneously from many directions, will be used to compress and heat the D-T gas mixture to levels necessary for fusion. In the targets studied here, the targets did not collapse, the x-rays did not go into the target, and a plasma was created which spread around the surface.

While a direct correlation may not be drawn between this study and those related to the controlled fusion program, some of the procedural and diagnostic techniques may prove valuable. The ability of a laser beam to focus accurately on a target of these dimensions was demonstrated by the team which conducted the experiment. The use of pinhole shadowgraphs and x-ray photographs was proven as an accurate measurement technique for the plasma dynamics on targets of this size. The plasma velocities calculated from these results agree with those found elsewhere in the published literature. These methods of remote measurement will be necessary since the targets will be too small, and temperatures and pressures too high, for readings by conventional probes.

Further studies of the damage mechanisms to spherical targets can be carried out. By using existing laboratory facilities at NPS, spherical targets of known composition could be irradiated at known background pressures. The intensity of each pulse could be measured, and probes could be used to measure the magnetic fields. Then the arc size and density distribution could be mapped and correlated with all of the above data to get a more quantitative model of the plasma dynamics for spherical targets.

APPENDIX A

TABLES

TABLE I

RADIAL TRANSPORT MEASUREMENTS FOR ASTERIX III IODINE LASER

Irradiance (10^{15} W cm^{-2})	6.0 ± 2.0
Wavelength (micrometers)	1.3
Pulse length FWHM (ps)	300
Fractional absorption	0.4
Local deposition (%)	1 ± 0.2
Remote deposition (%)	6 ± 1
Spreading Rates (10^{8} cm s^{-1})	3.5 ± 1.5

TABLE II

TARGET CRATERS

TARGET	SPHERE DIAMETER (micrometers)	CRATER DIAMETER (micrometers)	FIGURES
A	1000	337	B.6, E.6a
B	1000	524	B.7, E.7a
C	570	400	B.8, E.8a
D	570	250	B.9, B.9a
E	570	280	B.10, B.10a

TABLE III

HOT ELECTRON DEPOSITION ANALYSIS FROM X-RAY PHOTOGRAPHS

TARGET SIZE (micrometers)	ARC OF X-RAY EMISSION (degrees)	AREA OF DEPOSITION (m^2)	ENERGY FLUX DEPOSITED BY HOT ELECTRONS (W/cm^2)
1000	90 - 120	7.85×10^{-6}	3.8×10^{11}
450	90 - 180	3.18×10^{-7}	9.4×10^{12}
320	120 - 180	8.04×10^{-8}	3.7×10^{13}

TABLE IV

PLASMA VELOCITY DISTRIBUTIONS DERIVED FROM X-RAY PHOTOGRAPHS

TARGET (micrometers)	MAX RADIAL EXTENT (degrees)	DISTANCE (cm)	VELOCITY (cm/sec)
450	180	.071	2.4×10^8
1000	120	0.10	3.5×10^8

TABLE V

PLASMA VELOCITY DISTRIBUTIONS DERIVED FROM SHADOWGRAPHS

TARGET (micrometers)	DIST IN 1.9 nsec (mm)	VELOCITY (cm/sec)
570	7.1	3.8×10^6
1000	8.0	4.2×10^6

APPENDIX B
FIGURES

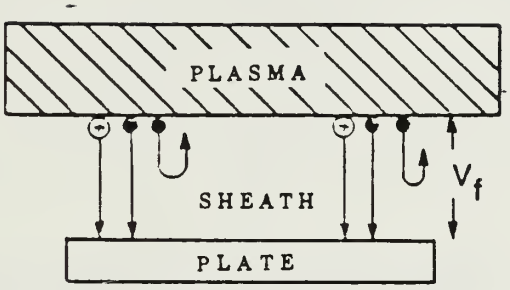

Figure B.1 Equilibrium Flow of Electrons and Ions to Isolated Plate.

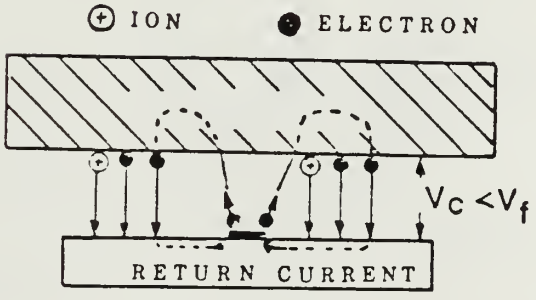

Figure B.2 Equilibrium Flow of Electrons and Ions to Isolated Plate with Electron Emission from a Cathode Spot.

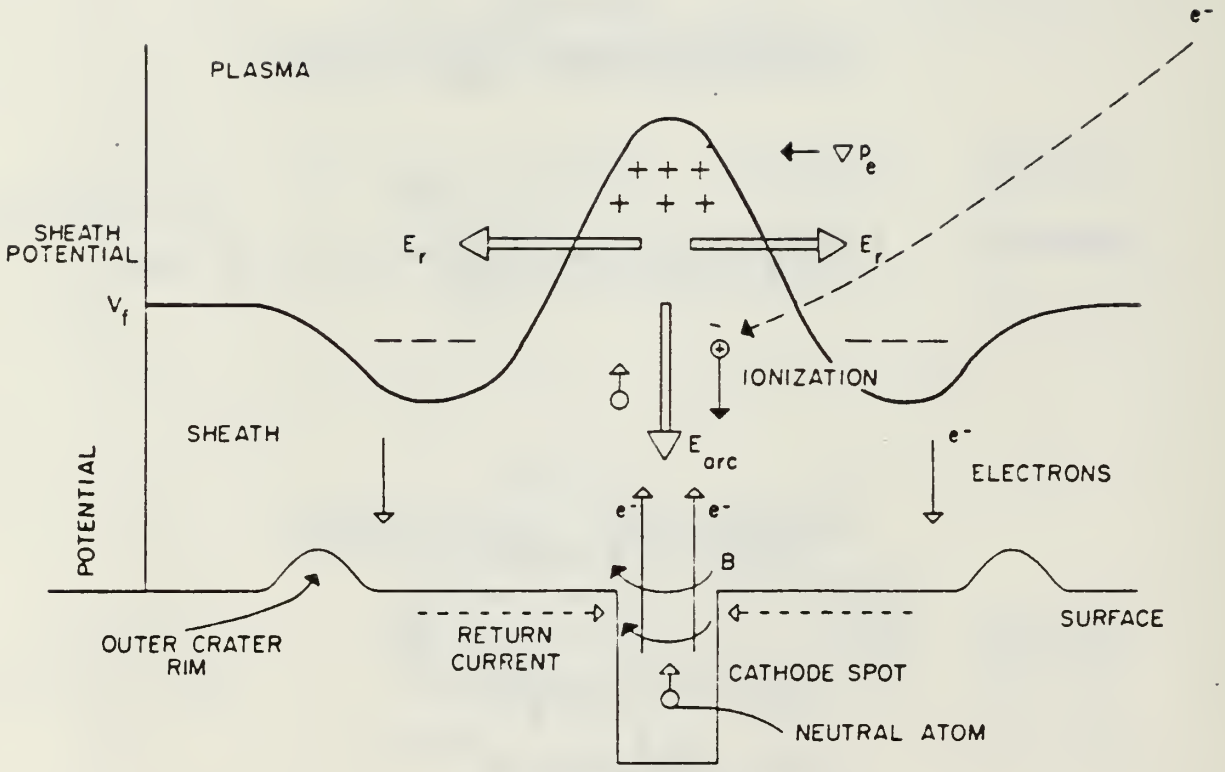

Figure E.3 Unipolar Arc Model.

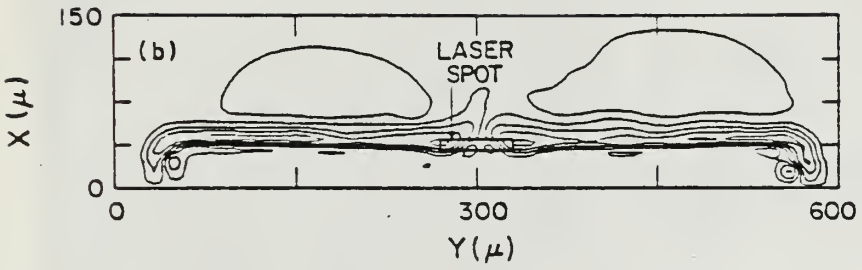

Figure B.4 Magnetic Field Lines Showing Propagation to Rear Surface of Target.

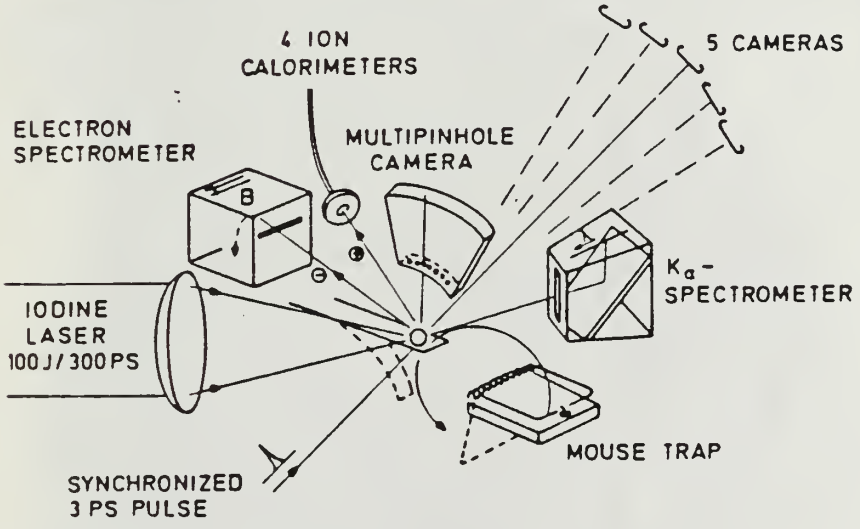

Figure B.5 Experimental Scheme With Diagnostic and Simple Apparatus for the Release of Free-Falling Targets.

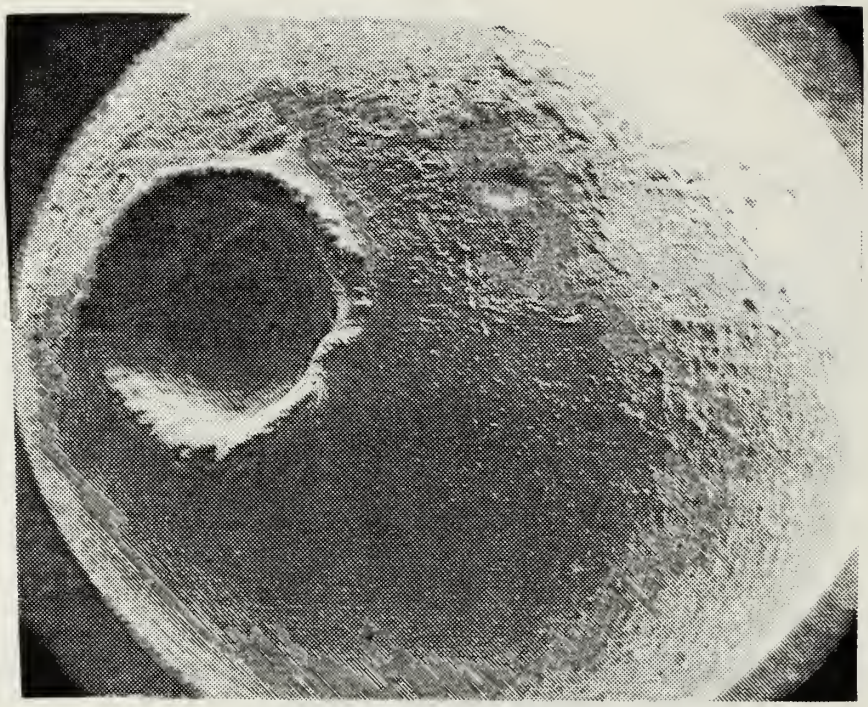

Figure B.6 Target A (X 100).

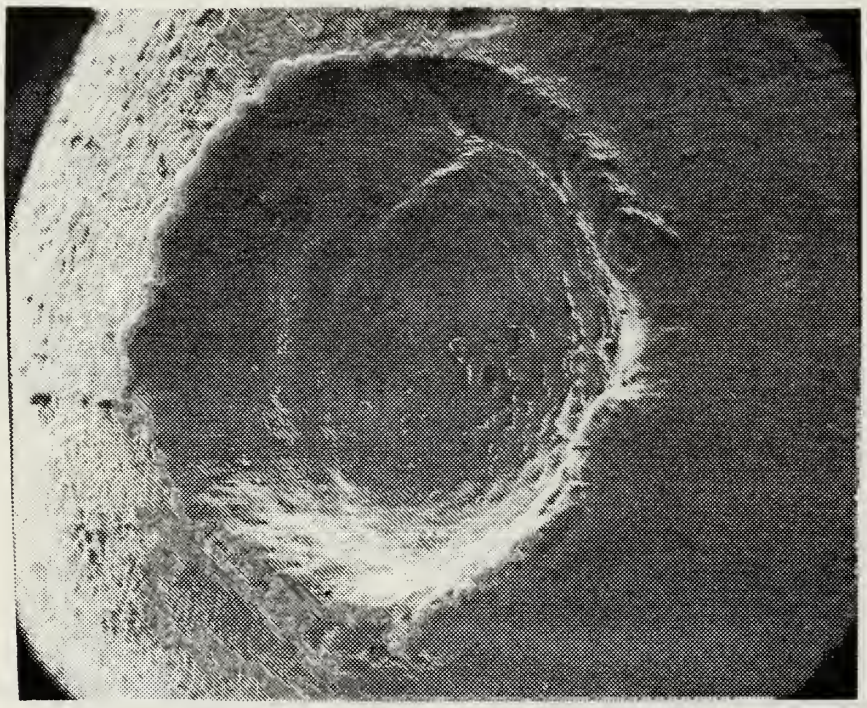

Figure B.6a Target A Crater (X 200).

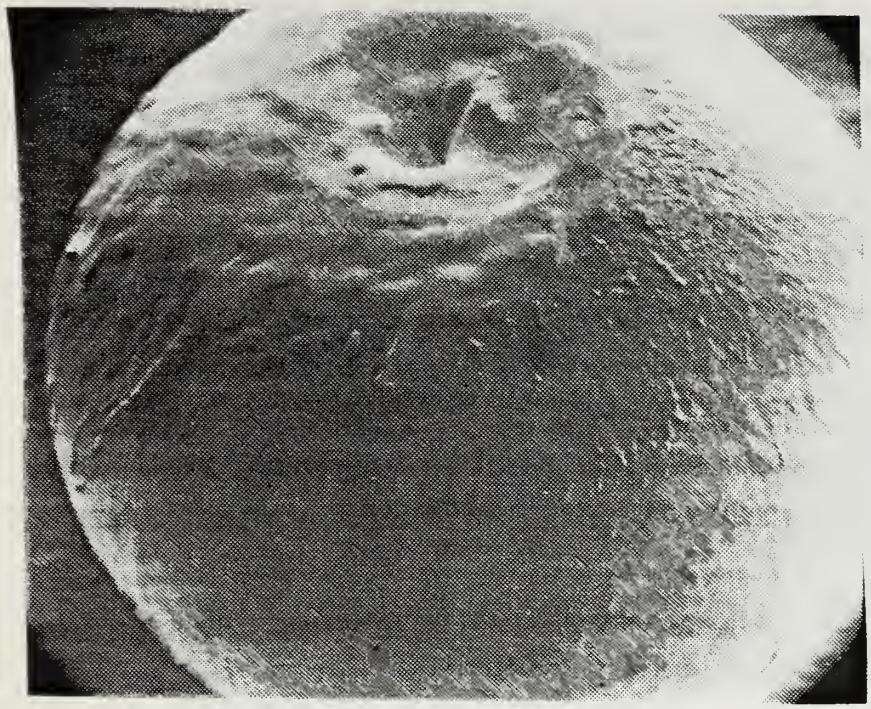

Figure B.7 Target B (X 100).

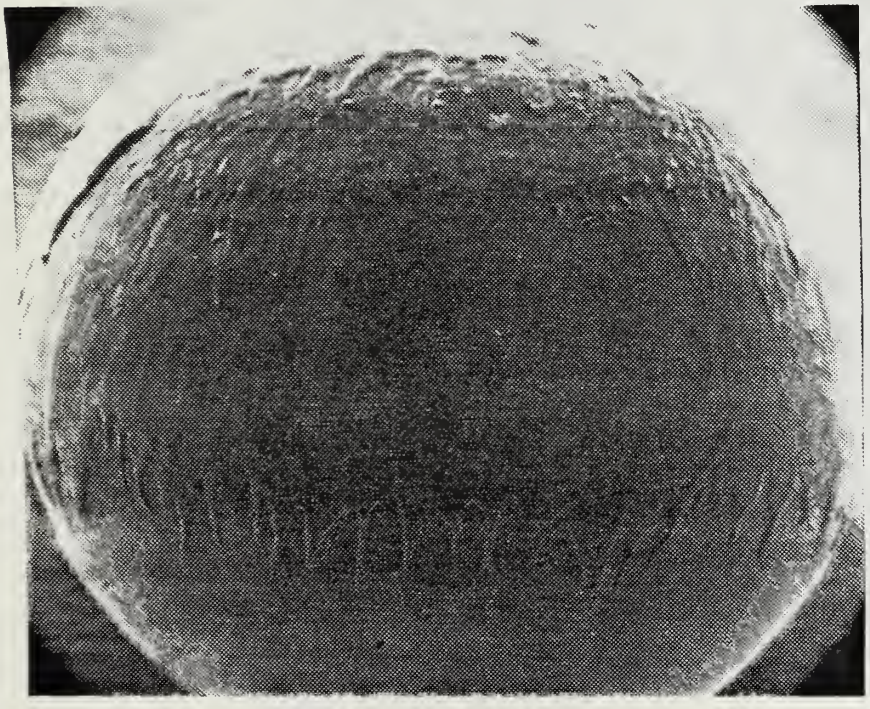

Figure B.7a Target B Profile (X 100).

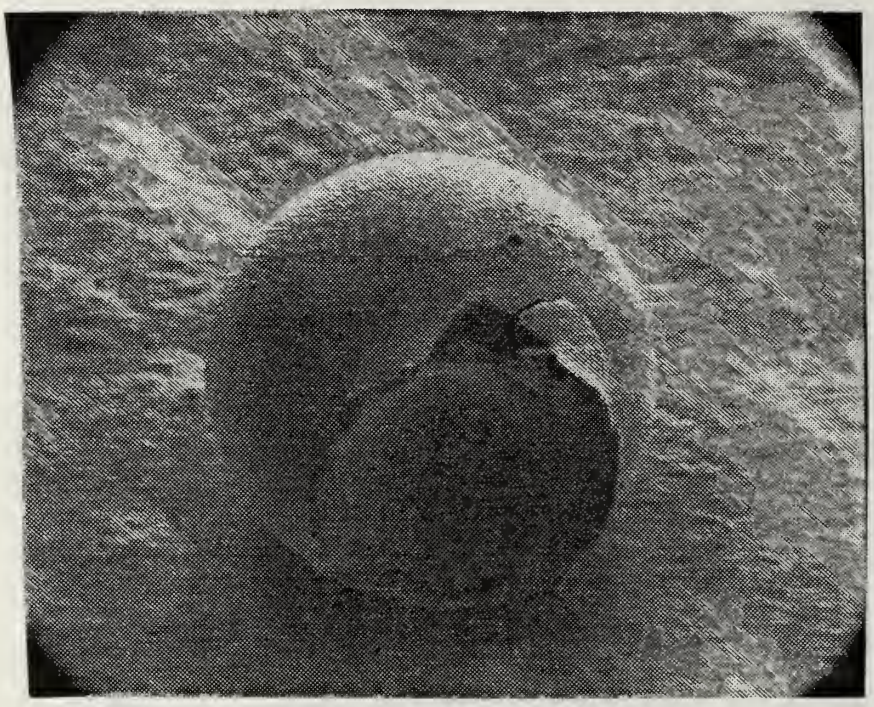

Figure B.8 Target C (X 100).

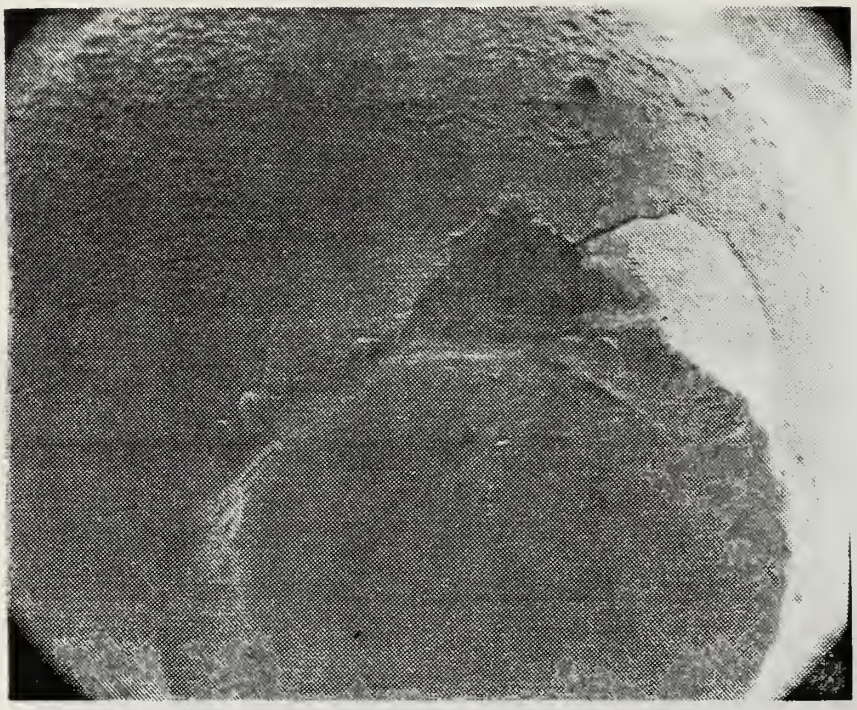

Figure B.8a Target C Crater (X 200).

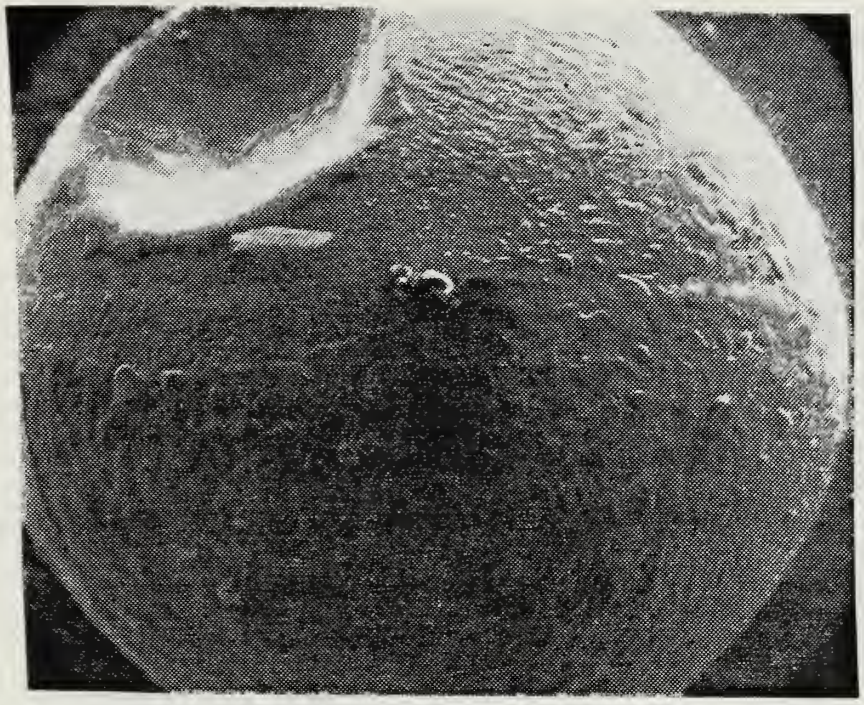

Figure B.9 Target D (X 195).

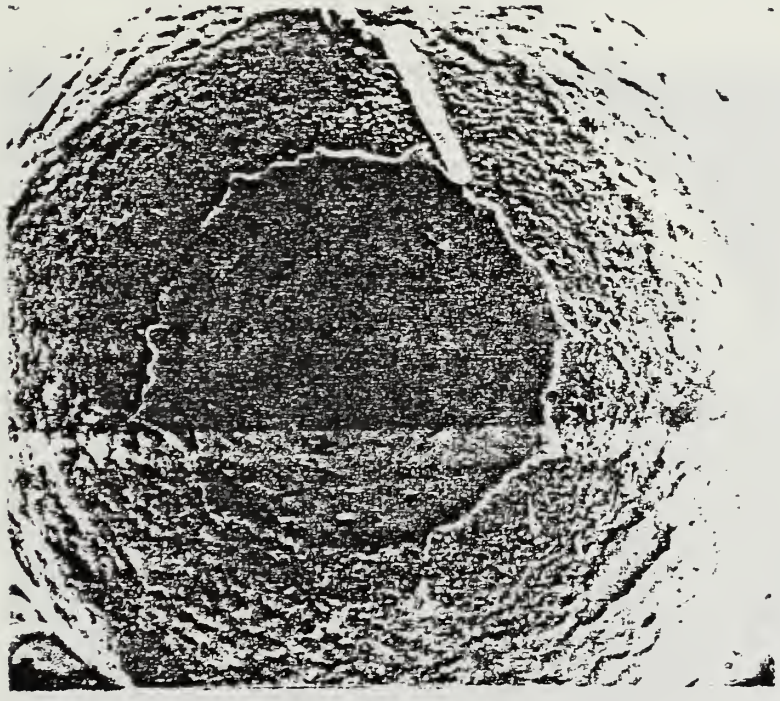

Figure B.9a Target D Crater (X 190).

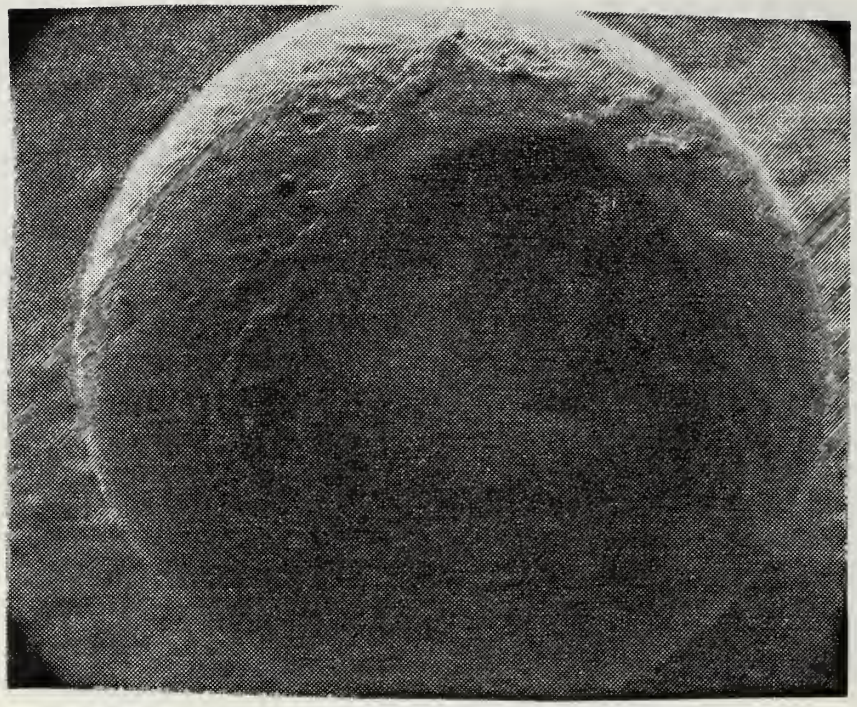

Figure B.10 Target E Crater (X 165).

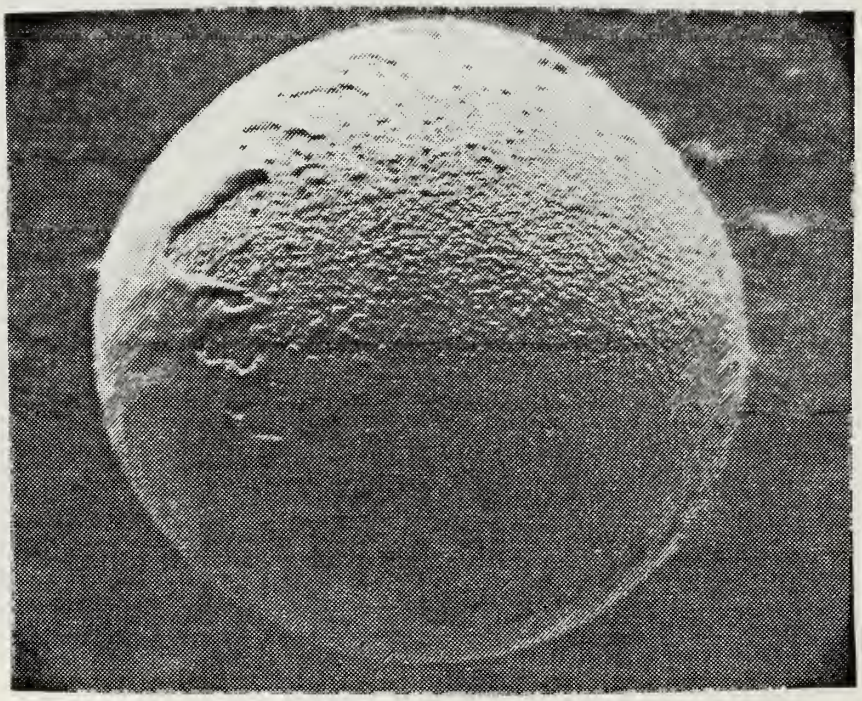

Figure B.10a Target E, 135 Degrees Off Shot Axis (X 145).

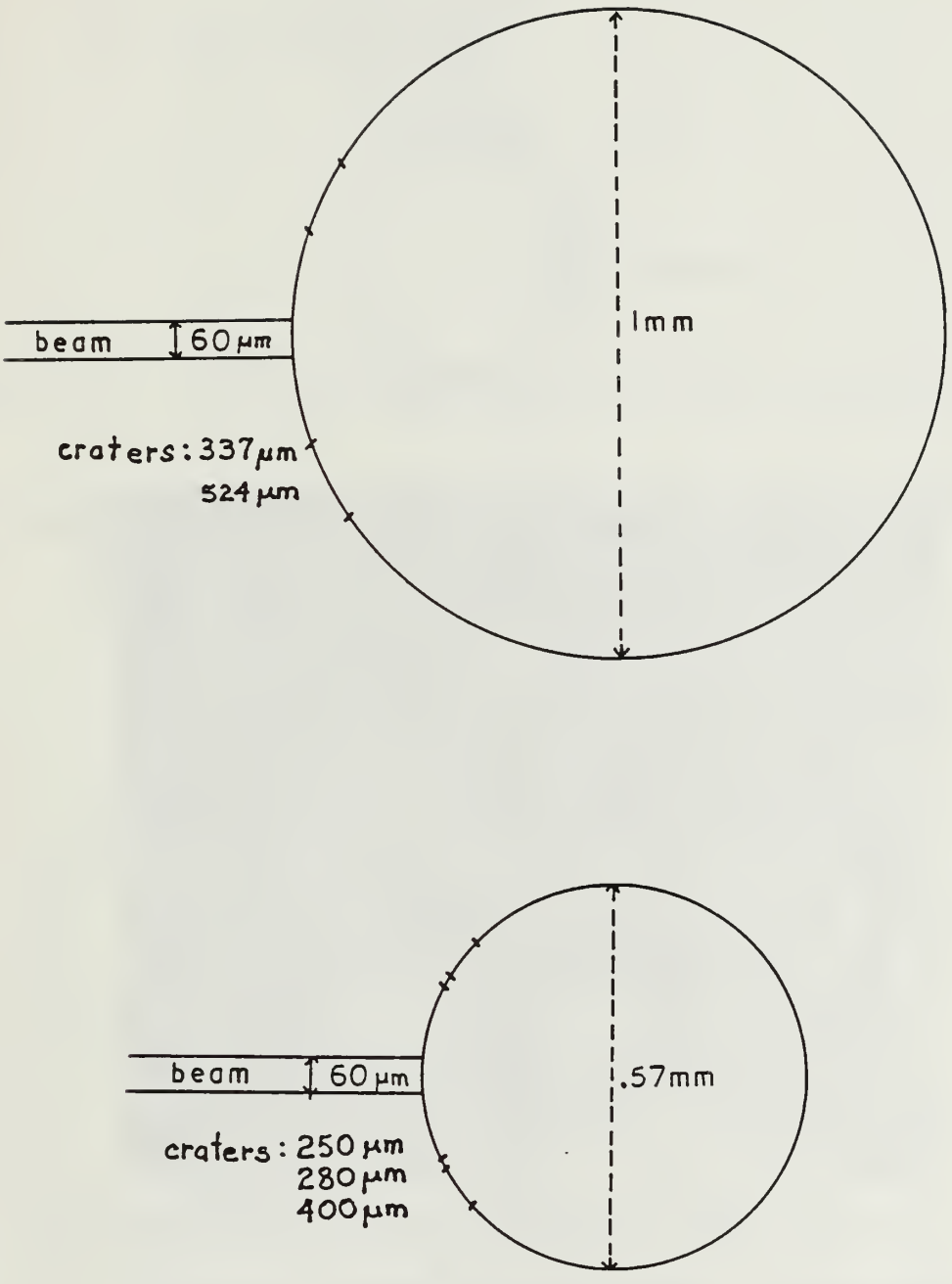

Figure B.11 Relative Dimensions of Laser Pulse, Crater and Sphere.

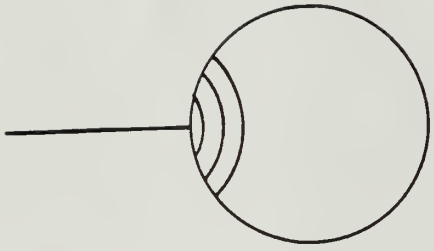

Figure B.12 Progressive Vaporization of Sphere by Laser Beam.

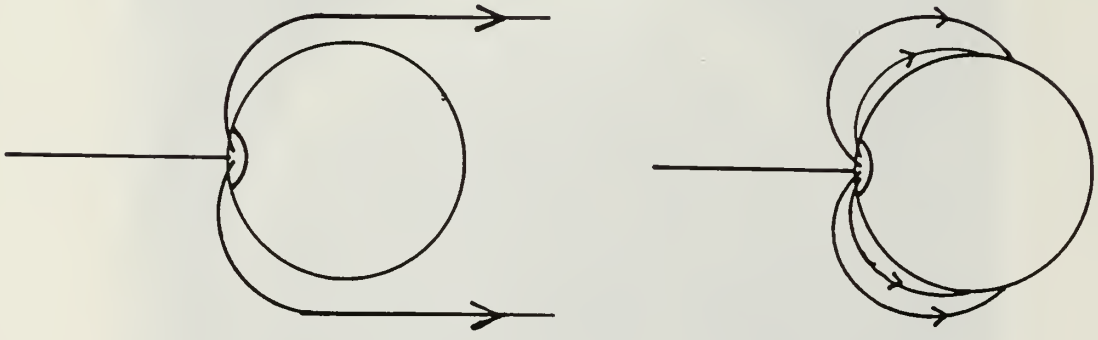

Figure B.13 Smooth Liquid Metal Flow (L)
Liquid Metal Debris (R).

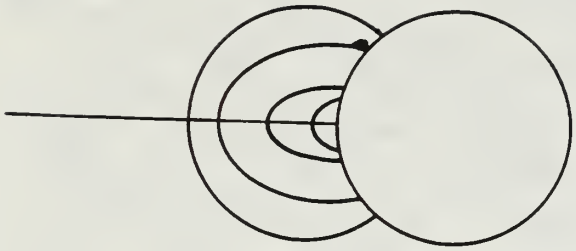

Figure B.14 Initial Plasma Expansion from a Laser Pulse.

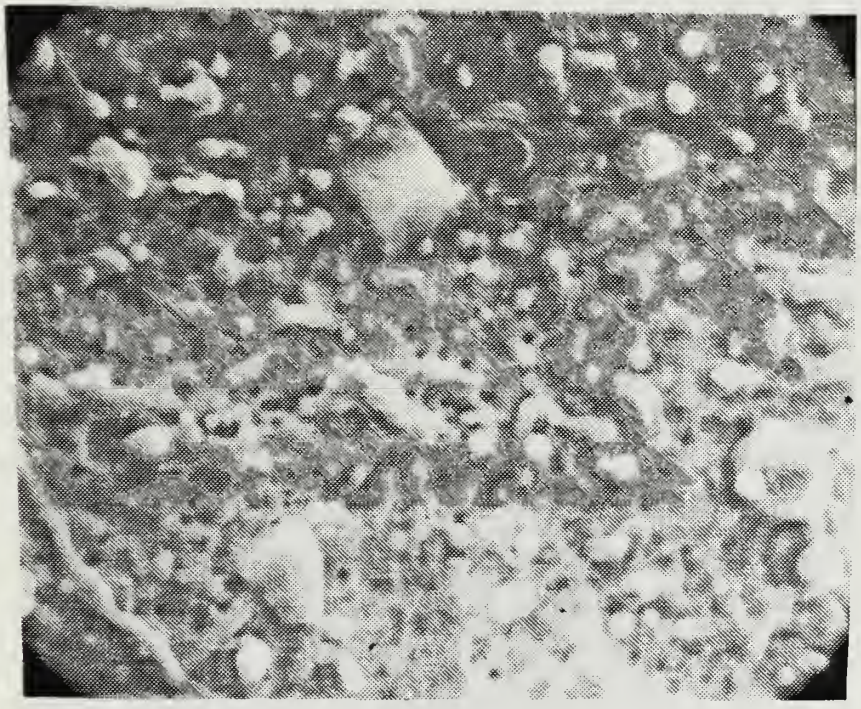

Figure B.15 Target A (X 2000)
Area Severely Damaged by Arcing (Note Debris).

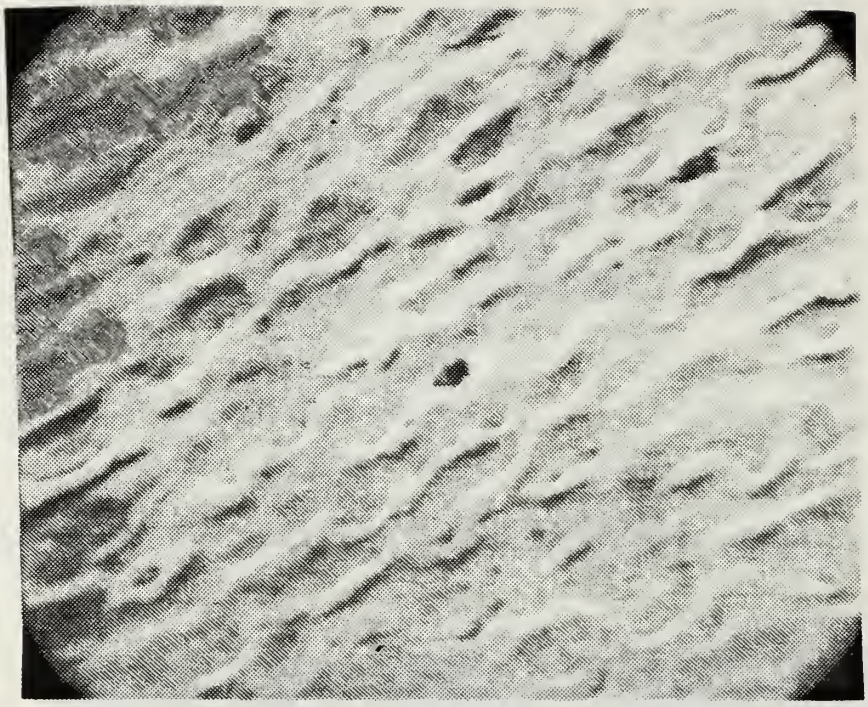

Figure B.16 Target B (X 2000)
Superposition of Several (5) Arcs in One Location.

Figure B.17 Target A, 90 - 100 Degrees Off Shot Axis (X 1000)
Note Smallness and Sparsity of Arcs.

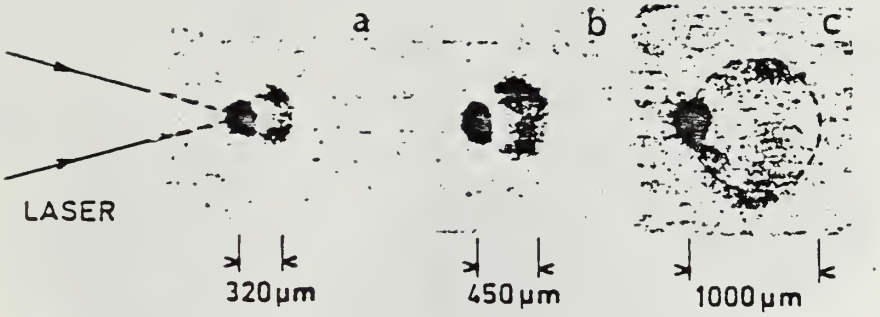

Figure B.18 X-ray Pinhole Photographs for .320, .450 and 1.00 mm Spheres.

Figure B.19 Time Resolved Shadowgraph for .450 mm Vanadium Sphere.

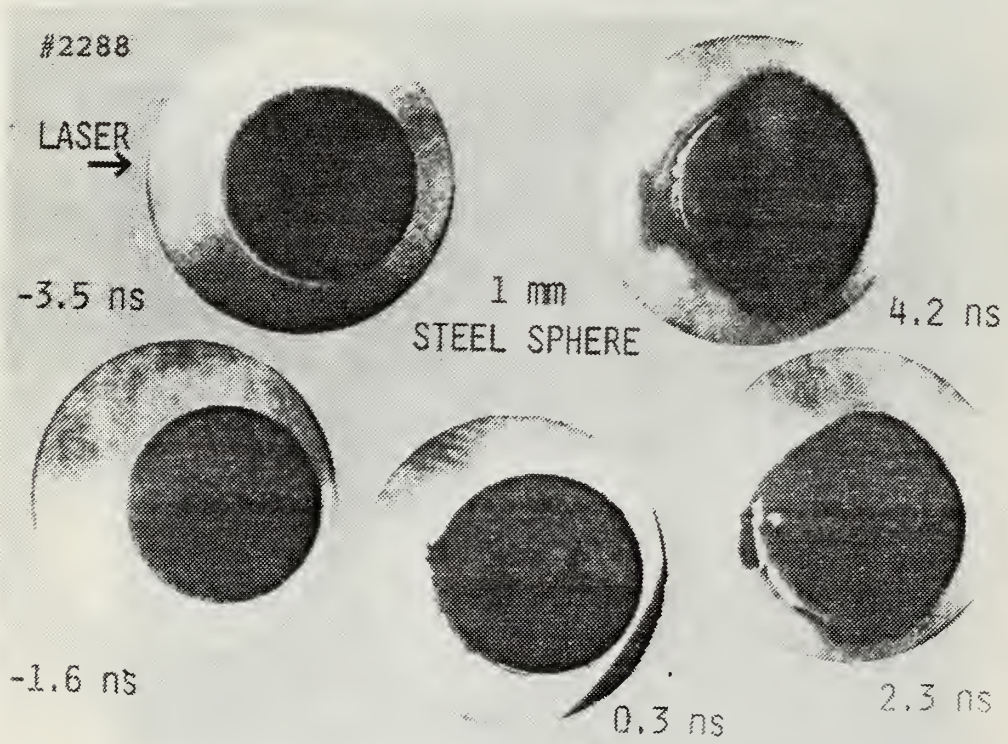

Figure B.20 Time Resolved Shadowgraph for 1.0 mm Steel Sphere.

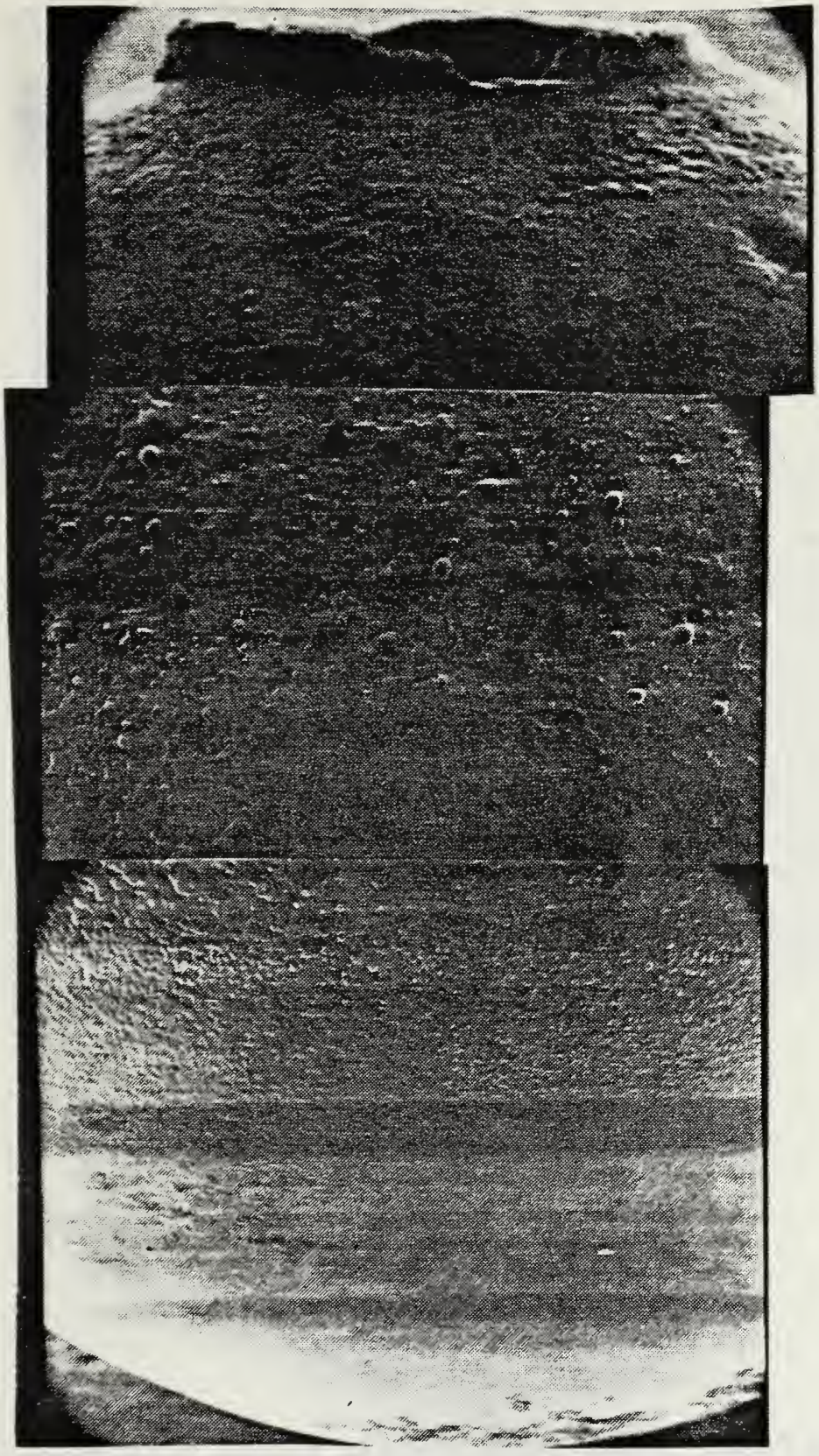

Figure B.21 Composite Profile of Target A (X 200)
Note Distribution and Flow of Damage.

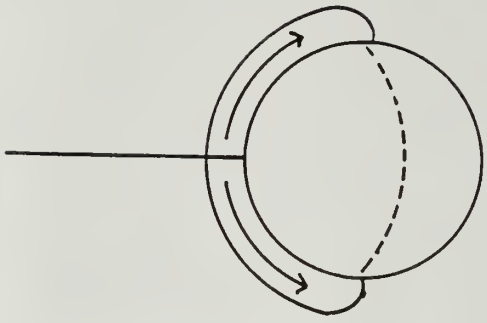

Figure B.22 Initial Plasma Flow for 1.00 mm Target.

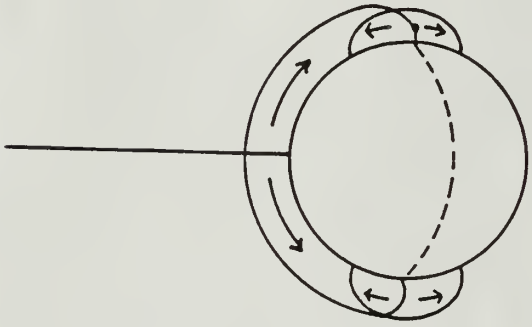

Figure B.23 Growth of Hot Electron Plasma at Equator of 1.00 mm Target.

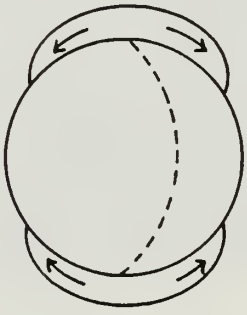

Figure B.24 Final Phase Showing Plasma Spread at Equator of 1.00 mm Target.

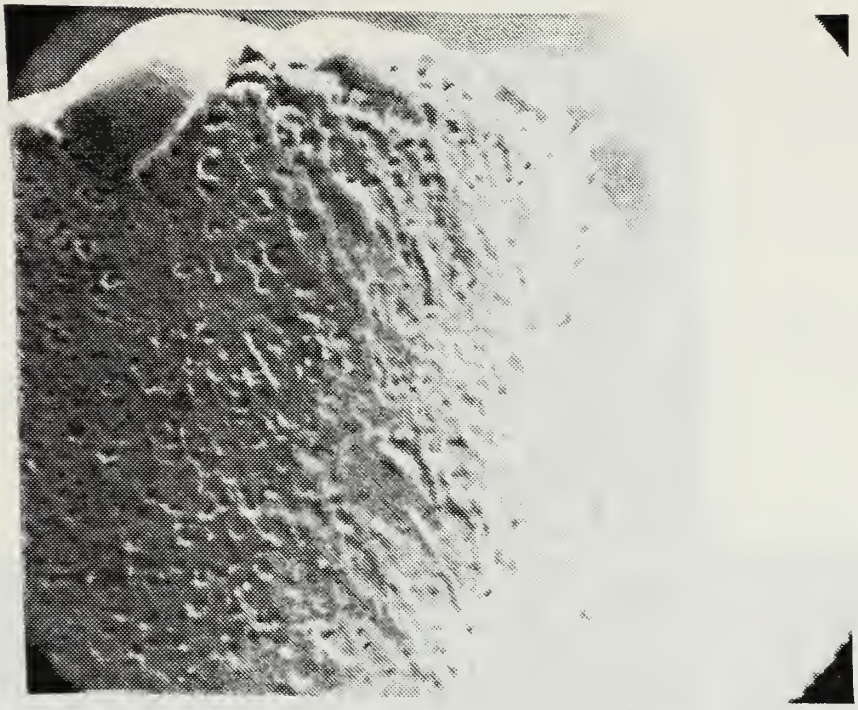

Figure B.25 Target C (X 1000)
Area just Outside Shot Crater.

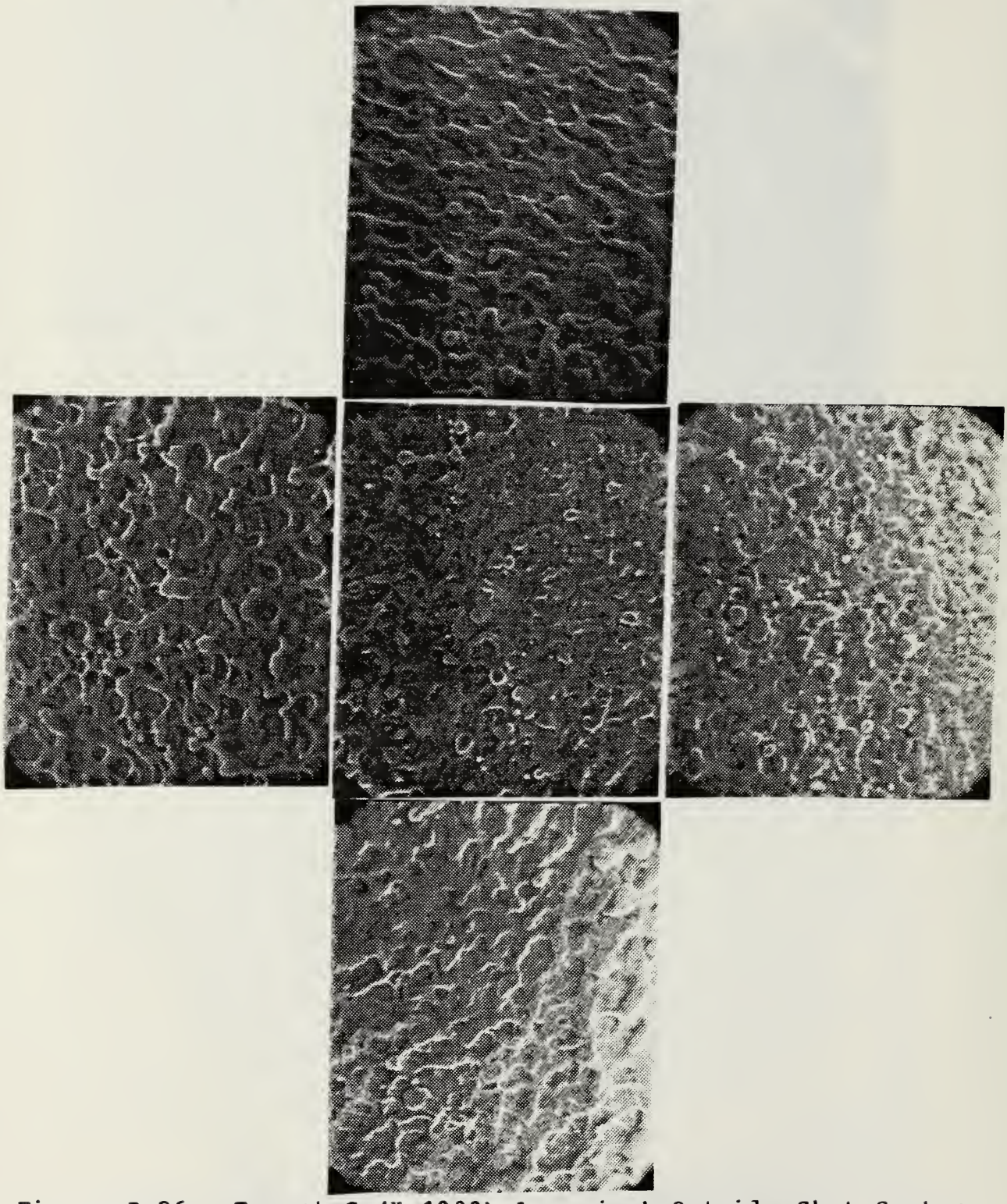

Figure B.26 Target C (X 1000) Area just Outside Shct Crater Center Photo at Pcle, Others 135 Degrees Off Shot Axis Note Flow Direction.

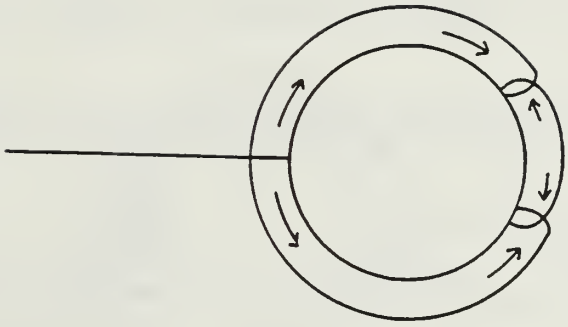

Figure B.27 Hot Electron Deposition and Magnetic Field of .570 mm Target.

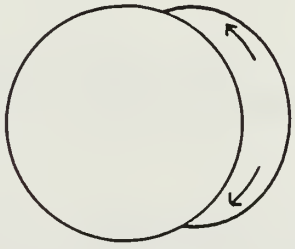

Figure B.27a Plasma Flow After Laser Pulse.

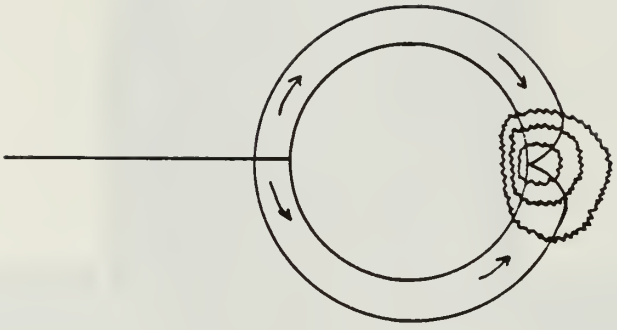

Figure B.28 Collision of Plasma Fronts at Rear Pole of Target Creating Shock Waves.

LIST OF REFERENCES

1. Linlor, W.I., "Ion Energies Produced by Laser Giant Pulses," Applied Physics Letters, v. 3, pp. 210-211, 1 December 1963.

2. Korobkin, V.V., and Seror, R.V., "Investigation of the Magnetic Field of a Spark Produced by Focusing Laser Radiation," JETP Letters, v. 4, pp. 102-106, 1 August 1966.

3. Stamper. J.A., Papadopoulos, K., Sudan, R.N., Dean, S.O., McLean, E.A., and Dawson, J.M., "Spontaneous Magnetic Fields in Laser-Produced Plasmas," Physical Review Letters, v. 26, pp. 1012-1015, 26 April 1971.

4. Eidmann, K., Maaswinkel, A., Sigel, R., Witkowski, S., Amiranoff, F., Fabbro, R., Hares, J.D., and Kilkenny, J.D., "Hot-electron Deposition Around Unsupported Laser Targets," Applied Physics Letters, v. 43, pp. 440-442, 1 September 1983.

5. Naval Postgraduate School Report NPS-61-83-008, Unipolar Arcing, A Basic Laser Damage Mechanism, by F. Schwirzke, 5 May 1983.

6. Ebrahim, N.A., Joshi, C., Villeneuve, D.M., Burnett, N.H., and Richardson, M.C. "Anomalous Energy Transport to Rear Surface of Microdisks at High Laser Irradiances", Physics Review Letters, v. 43, pp. 1995-1998, 31 December 1979.

7. Schwirzke, F., "Laser Induced Unipolar Arcing," Laser Interaction and Related Plasma Phenomena, v. 6, pp. 335-352, 1984.

8. Hares, J.D. and Kilkenny, J.D., "Measurement of Fast-Electron Energy Spectra and Preheating in Laser-Irradiated Targets," Physical Review Letters, v. 42, pp. 1216-1219, 30 April 1979.

9. Amiranoff, F., Eidmann, K., Sigel, R., Fedosejevs, R., Maaswinkel, A., Yung-lu Teng, Kilkenny, J.D., Hares, J.D., Bradley, D.K., MacGowan, B.J., and Goldsack, T.J., "The Evolution of Two-Dimensional Effects in Fast-Electron Transport From High-Intensity Laser-Plasma Interactions," Journal of Physics D, v. 15, pp. 2463-2468, 1982.

10. Forslund, D.W. and Brackbill, J.U., "Magnetic-Field-Induced Surface Transport on Laser-Irradiated Foils," Physical Review Letters, v. 48, pp. 1614-1617, 7 June 1982.

11. Schwirzke, F., "Measurements of Spontaneous Magnetic Fields in Laser-Produced Plasmas," Laser Interactions and Related Plasma Phenomena, v. 3, pp. 213-235, Plenum Press, 1974.

12. McKee, L.L., Bird, R.S., and Schwirzke, F., "Self-Generated Magnetic Fields Associated with a Laser-Produced Plasma," Physical Review A, v. 9, pp. 1305-1310, March 1974.

13. Sakagami, Y., Kawakami, H., Nagao, S., and Yamanaka, C., "Two-Dimensional Distribution of Self-Generated Magnetic Fields near the Laser-Plasma Resonant-Interaction Region," Physical Review Letters, v. 42, pp. 839-842, 26 March 1979.

14. Fabbro, R. and Mora, P., "Hot Electrons Behavior in Laser-Plane Target Experiments," Physics Letters A, v. 90A, pp. 48-50, 21 June 1982.

15. Rudie, Norman J., Principles and Techniques of Radiation Hardening, v. 3, Western Publishing Co., 1980.

BIBLIOGRAPHY

Benjamine, R.F., McCall, G.H., and Ehler, A.W., "Measurement of Return Current in a Laser-Produced Plasma," Physical Review Letters, v. 42, pp. 890-893, 2 April 1979.

Case, R.S. and Schwirzke, F., "Background Gas Pressure Dependence and Spacial Variation of Spontaneous Generated Magnetic Fields in Laser-Produced Plasmas," Journal of Applied Physics, v. 46, pp. 1493-1498, April 1975.

Drouet, M.G. and Boltcn, R., "Distribution of Self-Generated Current in Laser-Produced Plasmas," Physical Review Letters, v. 36, pp. 591-594, 15 March 1976.

Ehler, A.W., Begay, F., Tan, T.H. and Castine, P.H., "Lateral Transport of Energy from a Laser-Produced Plasma," Journal of Physics D, v. 13, pp. L65-L66, 1980.

Forslund, D.W., Kindel, J.M. and Lee, K., "Theory of Hot-Electron Spectra at High Laser Intensity," Physical Review Letters, v. 39, pp. 284-288, 1 August 1977.

Jaanimagi, P.A., Ebrahim, N.A., Burnett, N.H. and Joshi, C., "Return-Current Electron Streams in High-Intensity Laser Target Interaction," Applied Physics Letters, v. 38, pp. 734-736, 15 May 1981.

Kolodner, P. and Yablonovitch, E., "Two-Dimensional Distribution of Self-Generated Fields near the Laser-Plasma Resonant-Interaction Region," Physical Review Letters, v. 43, pp. 1402-1403, 5 November 1979.

Mitchell, K.B. and Godwin, R.P., "Energy-Transport Experiments in 10-micrometer Laser-Produced Plasmas," Journal of Applied Physics, v. 49, pp. 3851-3854, July 1978.

Morse, R.I. and Nielson, C.W., "Occurrence of High-Energy Electrons and Surface Expansion in Laser-Heated Target Plasmas," The Physics of Fluids, v. 16, pp. 909-920, June 1973.

Pert, G.J., "Self-Generated Magnetic Fields in Plasmas," Journal of Physics, v. 18, pp. 227-241, 1977.

Raven, A. and Willi, O., "Megagauss Magnetic Field Profiles in Laser-Produced Plasmas," Physical Review Letters, v. 41, pp. 554-557, 21 August 1978.

Schwirzke, F., Bunshah, R.F. and Taylor, R.J., "The Observation of Unipolar Arc Damage on Stainless Steel and TiC Coatings on Stainless Steel," Thin Solid Films, v. 83, pp. 117-123, 1981.

Slater, D.C., Busch, G.E., Charatis, G., Johnson, R.R., Mayer, F.J., Schroeder, R.J., Simpson, J.D., Sullivan, D., Tarvin, J.A. and Thomas, C.E., "Absorption and Hot-Electron Production for 1.05 and 0.52 Micrometer Light on Spherical Targets," Physical Review Letters, v. 46, pp. 1199-1202, 4 May 1981.

Yaakobi, B., Pelah, I. and Hoose, J., "Preheat by Fast Electrons in Laser-Fusion Experiments," Physical Review Letters, v. 37, pp. 836-839, 27 September 1976.

Yates, M.A., van Hulsteyn, D.B., Rutkowski, H., Kyrala, G. and Brackbill, J.U., "Experimental Evidence for Self-Generated Magnetic Fields and Remote Energy Deposition in Laser-Irradiated Targets," Physical Review Letters, v. 49, pp. 1702-1704, 6 December 1982.

Zigler, A. and Zmora, H., "The Origin of K* Radiation in Laser-Produced Aluminum Plasma," Physics Letters, v. 63A, pp. 275-277, 14 November 1977.

INITIAL DISTRIBUTION LIST

		No. Copies
1.	Defense Technical Information Center Cameron Station Arlington, Virginia 22304-6145	2
2.	Library, Code 0142 Naval Postgraduate School Monterey, California 93943-5100	2
3.	Professor F. R. Schwirzke, Code 61Sw Department of Physics Naval Postgraduate School Monterey, California 93943-5100	2
4.	Professor A. W. Cooper, Code 61Cr Department of Physics Naval Postgraduate School Monterey, California 93943-5100	1
5.	Lt. Charles O. Stephenson 3407 N. Pleasant Independence, Missouri 64050	1
6.	Department Chairman, Code 61 Department of Physics Naval Postgraduate School Monterey, California 93943-5100	1

25332

Thesis
S697 Stephenson
c.1 Laser damage to
spherical targets.